

Comparative Scanning Tunneling Microscopy Study on Hexaborides

Steffen Wirth,* Sahana Rößler, Lin Jiao,† and M. Victoria Ale Crivillero
Max Planck Institute for Chemical Physics of Solids, 01187 Dresden, Germany

Priscila F. S. Rosa
Los Alamos National Laboratory, Los Alamos, NM 87545, USA

Zachary Fisk
Department of Physics, University of California, Irvine, California 92697, USA
(Dated: October 26, 2021)

We compare STM investigations on two hexaboride compounds, SmB_6 and EuB_6 , in an effort to provide a comprehensive picture of their surface structural properties. The latter is of particular importance for studying the nature of the surface states in SmB_6 by surface-sensitive tools. Beyond the often encountered atomically rough surface topographies of *in situ*, low-temperature cleaved samples, differently reconstructed as well as B-terminated and, more rarely, rare-earth terminated areas could be found. With all the different surface topographies observed on both hexaborides, a reliable assignment of the surface terminations can be brought forward.

I. INTRODUCTION

The hexaborides of cubic structural type CaB_6 ($Pm\bar{3}m$) represent a very versatile class of compounds¹. LaB_6 features a very low work function of about 2.7 eV² while electron-doped CaB_6 is a ferromagnetic material, albeit with low magnetic moment^{3,4}, and CeB_6 exhibits quadrupolar ordering⁵. The hexaborides are often highly conductive. From Hall measurements it was shown⁶ that the majority of the hexaborides has one charge carrier per rare-earth atom, with the exceptions of divalent Eu and Yb with very low charge carrier densities and SmB_6 exhibiting intermediate valence^{7,8}.

The material SmB_6 has attracted special attention recently as it was proposed to host topologically non-trivial surface states⁹. This material falls into the category of so-called Kondo insulators^{10,11} in which the insulating properties are brought about by hybridization between conduction bands (here *d*-bands) and localized *f*-states. In consequence, a narrow gap opens up at sufficiently low temperatures (below the Kondo temperature T_K) while the *f*-electrons provide the strong spin-orbit coupling required for the development of topologically protected surface states predicted by band structure calculations¹²⁻¹⁴. Subsequently, considerable experimental effort was made to verify the topological nature of the surface states, in particular through angle-resolved photoemission spectroscopy (ARPES) with spin resolution^{15,16}. Though there is a consensus on the existence of a conducting surface state^{17,18}, its topological nature is a matter of ongoing debate. For instance, the surface states observed by ARPES measurements have been interpreted in terms of Rashba splitting¹⁹. One crucial aspect^{20,21}, namely a Γ_8 quartet ground state of the Sm f^5 configuration, has recently been observed experimentally²², but is in contrast to some band structure calculations^{13,23,24}. Here, the strong correlations of the Kondo insulator as well as its intermediate valence

complicate band structure calculations²⁵. An additional complication is the complex (001) surface of SmB_6 itself due to its polar nature²⁶. Because of the cubic structure of SmB_6 , *in situ* cleaved surfaces usually required for surface-sensitive techniques like ARPES or Scanning Tunneling Microscopy/Spectroscopy (STM/S) are often atomically rough or reconstructed²⁷⁻³⁰. But even in case of atomically flat surfaces the interpretation of the surface termination in STM is controversial^{31,32}. In an effort to make progress in this complex situation we here compare topographies obtained by STM on SmB_6 and EuB_6 . The latter material is interesting in its own right due to its complex band structure³³, ferromagnetic properties³⁴ and polaron formation³⁵. We note that a comparative study of YbB_6 , CeB_6 and SmB_6 , primarily based on ARPES results, was recently brought forward³⁶.

II. EXPERIMENTAL SECTION

Single crystals of SmB_6 and EuB_6 were grown by an Al flux method³⁷⁻³⁹. The orientation of the single crystals was checked by Laue diffraction. The lattice constants are $a = 4.133 \text{ \AA}$ for SmB_6 and $a = 4.185 \text{ \AA}$ for EuB_6 .

For STM investigations, two ultra-high vacuum (UHV) systems were used⁴⁰. A ^4He system allows for base temperatures below 5 K; if a heating stage is used the base temperature is typically $\sim 6 \text{ K}$ (a temperature sensor is incorporated into the heating stage). If not stated otherwise, the STM/STS data reported in the following were obtained at $\sim 6 \text{ K}$. Our ^3He -based system operates down to a base temperature of $\sim 0.3 \text{ K}$ and allows to apply magnetic fields up to 12 T perpendicular to the investigated surface. Electrochemically etched tungsten tips were used if not stated otherwise. Tunneling spectroscopy was conducted by using a lock-in technique and adding a small ac modulation voltage V_{mod} of 0.1 or 1.0 mV (depending on bias voltage V , see respective figure caption) with a frequency of 117 Hz to the bias voltage.

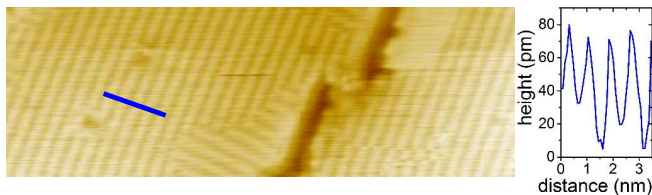


FIG. 1. Topography ($10 \text{ nm} \times 30 \text{ nm}$) of a reconstructed area of SmB_6 . Twinning between (2×1) and (1×2) reconstructions and dislocations of the reconstruction can clearly be seen ($V = 0.2 \text{ V}$, $I_{\text{sp}} = 0.5 \text{ nA}$). The height scan (right) was taken along the blue line indicated in the topography.

Some of the STM data reported in the following were obtained in a so-called dual-bias mode. In these cases, two different bias voltages V were applied for the forward and backward scan of the fast scan direction. This mode of operation allows to obtain topographic images with two different V at the same sample position (within the piezoelectric hysteresis of the scanner, typically giving offsets well below 1% of the total scan size of the two topographies). In doing so, drift corrections can be neglected and parameters like temperature T or magnetic field, sample history, surface termination, or tip condition are identical. Even if the tip changes, it then influences the data for both V at very similar sample positions.

All samples reported here were cleaved *in situ* along a (001) crystallographic plane at a temperature of $\sim 20 \text{ K}$ using identical cleaving stages in both UHV systems. After cleaving, the sample needs to be transferred into the respective STM head during which time (in the order of 10 s) the sample temperature is not controlled. We here provide results based on 24 cleaves of SmB_6 (on 8 of which we did not find any atomically flat surface area) and 5 cleaves on EuB_6 .

III. RESULTS

A. SmB_6

In order to obtain information on the nature of the surface states the applied probe needs to be surface sensitive. One obstacle in investigating SmB_6 with highly surface-sensitive tools like ARPES or STM are the different surface terminations. Due to the cubic structure of the hexaborides, the majority of the cleaved surface areas is rough on an atomic scale³¹. This may result in a modified local structure which, in turn, may influence the properties (specifically of Sm) at the surface^{41,42}.

Upon searching, a (2×1) surface reconstruction can usually be found^{28,30,43}. The (2×1) reconstruction was also observed by low-energy electron diffraction^{36,44,45} as well as by STM on LaB_6 ⁴⁶. Clearly, if we assume that the (2×1) reconstruction results from each second row of Sm atoms missing on top of an otherwise B-terminated surface, such a reconstruction is energetically favorable

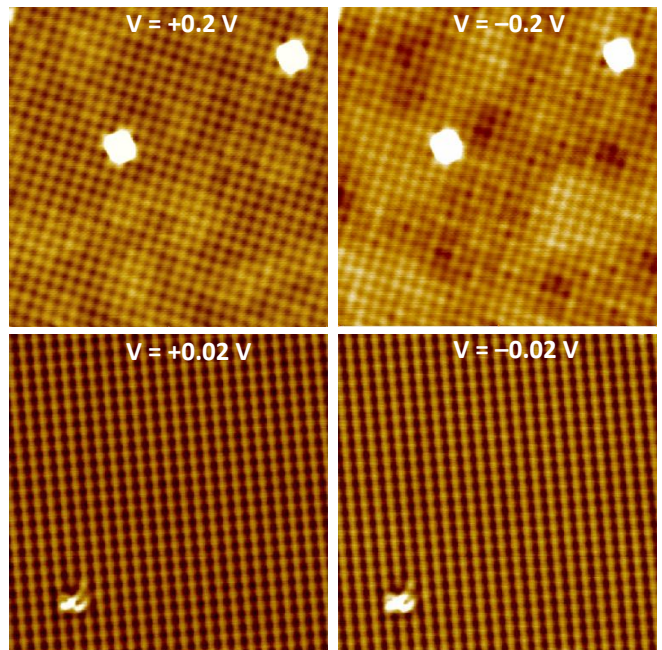


FIG. 2. The upper and lower row show two different SmB_6 topographies of areas $10 \text{ nm} \times 10 \text{ nm}$, both obtained in dual-bias mode: upper row $V = +0.2 \text{ V}$ (left) and $V = -0.2 \text{ V}$ (right), $I_{\text{sp}} = 0.6 \text{ nA}$; lower row $V = +0.02 \text{ V}$ (left) and $V = -0.02 \text{ V}$ (right), $I_{\text{sp}} = 0.3 \text{ nA}$. Images in the upper (lower) row were obtained at $\sim 6 \text{ K}$ ($\sim 1.7 \text{ K}$) and cover a total height scale of 155 pm (90 pm). Also the defects indicate that exactly the same sample areas are imaged on the left and right side, respectively.

compared to an unreconstructed polar surface. Yet, other STM studies did not report this reconstruction²⁹ or interpreted it differently³². It should also be noted that such a reconstruction may have repercussions on the metallic surface state⁴⁷.

In Fig. 1 we present such a (2×1) reconstructed surface area. The height scan taken along the blue line as indicated in the topography is consistent with the aforementioned idea of each second row of Sm atoms missing. This is corroborated by a change in height on and between these rows of atoms of the order 40–50 pm; yet, an order of magnitude smaller height oscillations for the (2×1) reconstructed surface was also reported^{30,43}. The reconstruction is likely formed during the cleaving process or subsequently upon some additional diffusion of surface atoms. In both cases, one may expect domains of (2×1) and (1×2) reconstructed areas and dislocations between the Sm rows by one lattice constant, both of which can easily be recognized in the topography, Fig. 1.

Rarely we also found atomically flat surface areas as shown in Fig. 2. Similar surface topographies have been presented before^{27–29,32,43,48,49}. It was shown, however, that the obtained topography depends on applied bias voltage V , and even a contrast reversal was observed for $V = 0.2 \text{ V}$ and -3.0 V ³². In the following we make use of the dual-bias mode described in Section II as it allows to

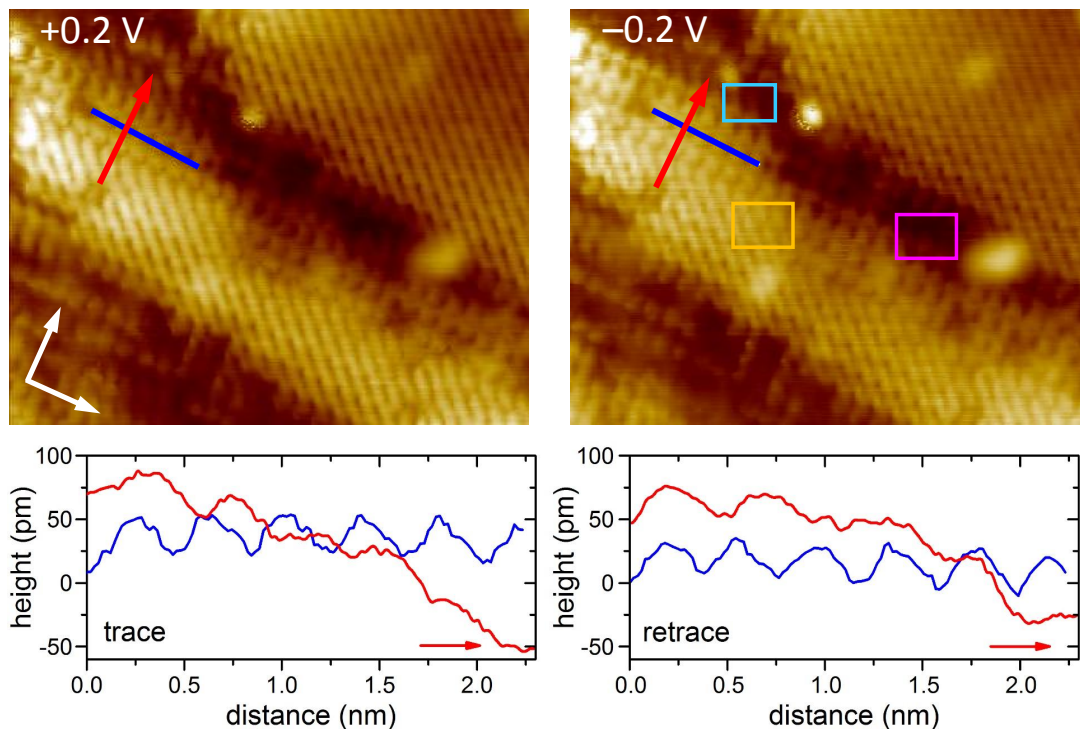


FIG. 3. SmB_6 topography of an area of $10 \text{ nm} \times 8 \text{ nm}$ exhibiting both Sm- and B-terminated areas. The images were obtained in dual-bias mode: $V = +0.2 \text{ V}$ (left) and $V = -0.2 \text{ V}$ (right). The height scans were taken along the lines of corresponding color in the topography images. Along the direction of the red arrows the sample height decreases by about $100 - 130 \text{ pm}$. The white arrows indicate the main crystallographic directions $\langle 100 \rangle$ and $\langle 010 \rangle$, respectively. The colored rectangles indicate the areas over which the spectroscopy curves of corresponding colors in Fig. 4 were averaged.

visualize exactly the same surface area without relying on defects on top of the investigated surface (the appearance of defects may change with V , see Fig. 2). We have chosen values of V small compared to the barrier height Φ (see also below) yet larger than the hybridization gap of less than 20 meV ^{29,50–54}. In Fig. 2 dual-mode topographies for $V = \pm 0.2 \text{ V}$ (upper) and $\pm 0.02 \text{ V}$ (lower) are compared. Note that here different samples were investigated at somewhat different temperatures of $T \sim 6 \text{ K}$ (upper) and 1.7 K (lower). Qualitatively, the topographies for given temperature agree very well, i.e. there is no contrast inversion of reversed V . There are subtle inhomogeneities in the background at $T \sim 6 \text{ K}$; we can only speculate that they result from a not fully developed conducting surface state because we so far did not observe such inhomogeneities at $T \leq 1.7 \text{ K}$ (see also discussion of Fig. 7 below). We note that very similar inhomogeneities are reported on atomically flat surfaces, Fig. S1B in³⁰.

To investigate the surface termination in more detail we present in Fig. 3 topographies on areas exhibiting steps of less than one unit cell height a ²⁸. Such steps are perfectly suited to gain information about the different surface terminations. Again, the topographies obtained in dual mode with $V \pm 0.2 \text{ V}$ agree on a qualitative level. The white arrows in Fig. 3 indicate the main crystallographic directions $\langle 100 \rangle$ and $\langle 010 \rangle$. Height scans taken along the blue lines, i.e. parallel to one of the main crys-

tallographic directions and at overall unchanged height, clearly indicate lateral distances between corrugations consistent with the lattice constant a , while such taken along descending height (red arrows) exhibit less obvious corrugations (possibly related to crystallographic imperfections within such regions of changing overall height). Within elevated areas (bright regions), however, the corrugations appear to run along the diagonal, i.e. $\langle 1\bar{1}0 \rangle$, directions. This is consistent^{27,28} with a Sm-terminated surface where also, in addition to the Sm atoms, the apex atoms of the B-octahedra are seen, see discussion of Fig. 8 below as well as the crystal structure shown in Fig. 4.

We now turn to the height scans taken along the red arrows in the topographies which, again, follow a $\langle 100 \rangle$ direction but also include a height change. Atomic distances corresponding to a can be seen for $V = +0.2 \text{ V}$, but less well for $V = -0.2 \text{ V}$. Clearly, the total change in height depends to some extent on V : It amounts to about 130 pm for $V = +0.2 \text{ V}$ and $\sim 100 \text{ pm}$ for -0.2 V . Yet, both numbers appear to be consistent with the expected step height upon going from a Sm- to a B-terminated surface considering the inter-octahedron B distance of 164.6 pm . Given the fact that distances of a are observed along the main crystallographic directions on this (001) plane such a step height is difficult to interpret otherwise; a viable alternative is the opposite assignment (i.e. going from a B-terminated surface down to a Sm-

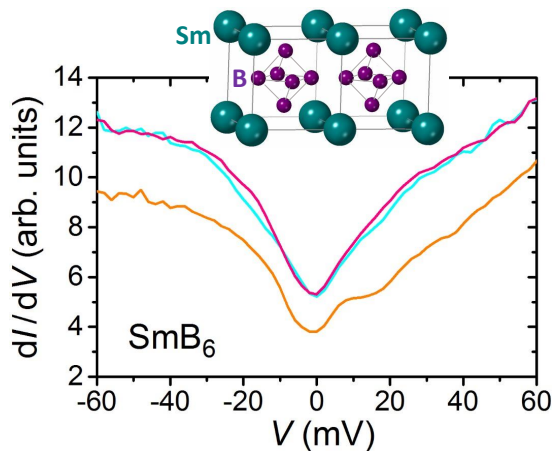


FIG. 4. Tunneling spectroscopy averaged over the areas marked by rectangles of corresponding colors in Fig. 3 (right). $V = +0.2$ V, $I_{sp} = 0.6$ nA, $V_{mod} = 1$ mV. The inset exhibits two adjacent unit cells of the cubic SmB_6 lattice.

terminated one) which would, however, involve breaking up of B-octahedra, i.e. intra-octahedral bond breaking. Estimates of the surface energy^{29,31} indicate a slight preference for inter-octahedral bond breaking but impurities or sample inhomogeneities and defects may change these estimates locally. Indeed, a donut-like structure was interpreted as breaking inter-octahedral bonds²⁷.

In order to gain further insight into the different terminations exposed in Fig. 3 tunneling spectroscopy was conducted. The STS curves shown in Fig. 4 correspond in color to the areas marked in Fig. 3 (right) over which the spectra were averaged. These spectra can be compared to those obtained on small areas of atomically flat surfaces, but differ from those seen on larger areas in that there is no pronounced maximum in dI/dV at around -20 mV²⁸. The orange spectrum attained on the elevated part of the topography Fig. 3 exhibits a well developed hump at $V \sim +10$ mV^{27,28,45}. It is tempting to compare this

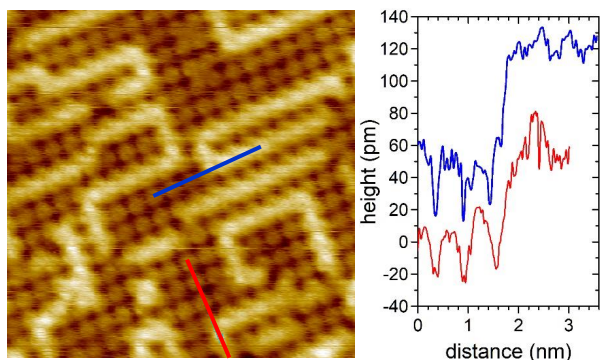


FIG. 5. Disordered reconstructed surface area (10 nm \times 10 nm) of SmB_6 . From the height profiles (taken along the lines of corresponding colors in the topography) the apparent height of the bright atoms is on the order of 60 pm ($V = +0.2$ V, $I_{sp} = 0.6$ nA, blue profile offset by 50 pm).

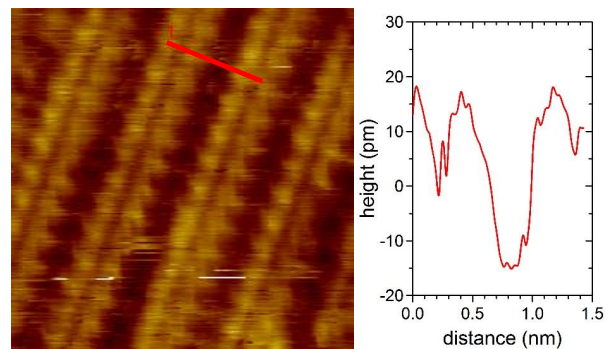


FIG. 6. Surface area (5 nm \times 5 nm) of SmB_6 within which only every third row of Sm appears to be missing ($V = +0.2$ V, $I_{sp} = 0.6$ nA). Right: height scan along the red line shown in the topography.

hump to the conspicuous maximum observed on Sm-terminated surface of larger areas^{27,28}. Note that we did not observe (Fig. 4 and²⁸) a pronounced shift in energy of features at negative V as reported elsewhere⁴⁹.

The discussion above indicated that a (2×1) reconstruction is energetically favorable with respect to the polar nature of a Sm- or B-terminated surface. However, a similar effect is conceivable if the (2×1) reconstruction is not long-ranged, but realized only locally. The lines of Sm may then meander^{28,31} not giving rise to a superstructure⁵². Part of such a “disordered” reconstructed surface is shown in Fig. 5. In such a case, a similar change in height upon going from the topmost Sm atoms to the underlying B layer is expected as in Fig. 3. The height scan, Fig. 5 (right), along the red line marked in the topography indeed supports this assertion.

In one instance, we observed a topography as presented in Fig. 6. The height scan may be interpreted as every third row of atoms missing. Here, the height change between the upper and lower rows of atoms is only about 30 pm, similar to²⁸ or slightly smaller (Fig. 1) than the case of (2×1) reconstructions. The exact number, however, may depend on details of the tip, i.e. how well it may penetrate between the rows of atoms, and may even be much smaller^{30,43}.

It should be noted again that our assignment of Sm- or B-terminated surfaces depends largely on the exact cleave, i.e. whether inter- or intra-octahedral bonds are broken. Albeit the former is, as mentioned above, energetically favorable, the latter may also occur as suggested by the observation of so-called donuts^{27,31}.

In Fig. 7 we present a topography over an area of 40 nm \times 40 nm. While we have certainly encountered areas showing a smaller number of defects⁴⁸ it provides an overview of the different types of defects found on a B-terminated surface. The largest protrusions, #1 (red) and #7 (dark blue) in the upper right panel, with heights well beyond 100 pm are most likely caused by adatoms on top of the surface. The short red dashes in the height scan mark distances of a suggesting that the underly-

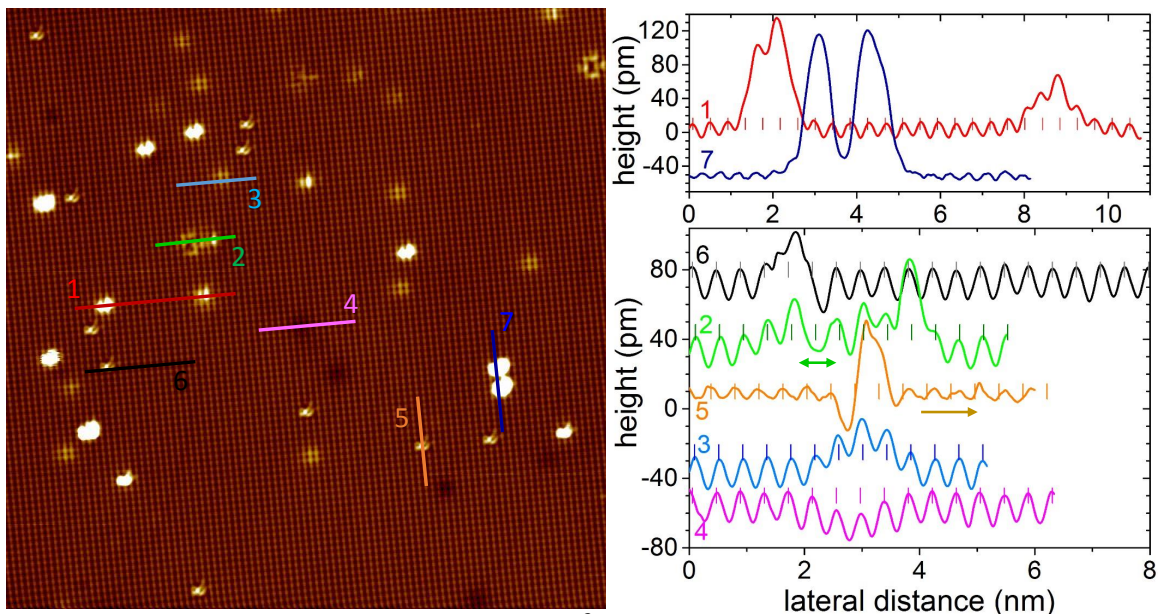


FIG. 7. Left: SmB_6 topography of a B-terminated area of $40 \text{ nm} \times 40 \text{ nm}$ with different types of defects ($V = 0.015 \text{ V}$, $I_{\text{SP}} = 0.3 \text{ nA}$, $T \approx 1.7 \text{ K}$). Right: Height scans taken along the lines of corresponding numbers and colors in the topography image. The dashes mark distances of one lattice parameter to indicate the expected atomic positions.

ing lattice is not disturbed beyond the defects. Other defects, #5 (orange) and #6 (black) in the lower right panel, appear to be incorporated into the lattice as also the immediate lattice sites seem influenced. Albeit conceivable, there is no evidence for an exchange of B by Al in pure SmB_6 ⁵⁵ (note that this refers to substitution of individual B atoms by Al, not to Al inclusion of non-negligible size^{56,57}). In the Th-Pd-B system it was found that Pd may replace two adjacent B atoms belonging to neighbouring octahedra⁵⁸. Along the same line one may speculate that a similar replacement of adjacent B atoms by impurities near the surface may result in the observed slight displacement of surface atoms. Qualitatively different are the defects #3 (light blue) and #4 (magenta). Here, the lateral position (again, the vertical dashes indicate distances of a) and the height oscillation of the protrusions appear to remain unchanged while the height level is either raised (#3) or lowered (#4) by about 15–20 pm over distances of about 2 lattice constants from the center of the defect. We speculate that the defect itself is located in a subsurface layer, possibly on a Sm site, leaving the B-octahedra intact. It should be noted that this type of defect seems qualitatively different from the background inhomogeneity of Fig. 2. Albeit a clear assignment of either one of these features to structural or electronic inhomogeneities is speculative at present, it is obvious that a clean surface is a prerequisite for their observation. It should also be noted that dents of about 80 pm have so far only been observed on Sm-terminated surfaces²⁸. The topography of such dents is very similar to the surface structure of La-terminated LaB_6 where La atoms are missing from the topmost layer⁵⁹. Therefore, it should be highly instructive to investigate Sm-

deficient samples $\text{Sm}_{1-x}\text{B}_6$ and attempt to correlate the Sm-deficiency x with the occurrence of these dents.

B. EuB_6

In contrast to SmB_6 , the ferromagnetic semimetal EuB_6 has so far only scarcely been investigated by STM³⁵ even though its electronic structure is not fully understood, see^{33,60} and references therein. Hence, STS—in particular by using a spin-polarized tip—may provide fresh insight. In the following, we focus on the surface topography.

In Fig. 8 we compare the topographies of rare-earth terminated samples EuB_6 and SmB_6 . In both cases, atomically flat and clean surface areas could be found after cleaving. The blue lines in the topographies indicate where the height scans parallel to the crystallographic $\langle 100 \rangle$ directions were taken. The corrugations of heights 30–40 pm are spaced apart by one respective lattice constant a . However, at the center of the square arrangements of these main corrugations in the topography (resulting from the cubic structure) additional humps are seen, also forming a regular, square arrangement. This is evidenced by the red height scans along the diagonal $\langle 110 \rangle$ directions, with the distances between the main and the interjacent smaller corrugations corresponding to $a/\sqrt{2}$. Based on the distances and orientations, the higher protrusions were assigned^{27,28} to the rare-earth atoms and the smaller ones to the apex of the B octahedra, again assuming breaking inter-octahedral bonds upon cleaving. We emphasize that the observation of in-

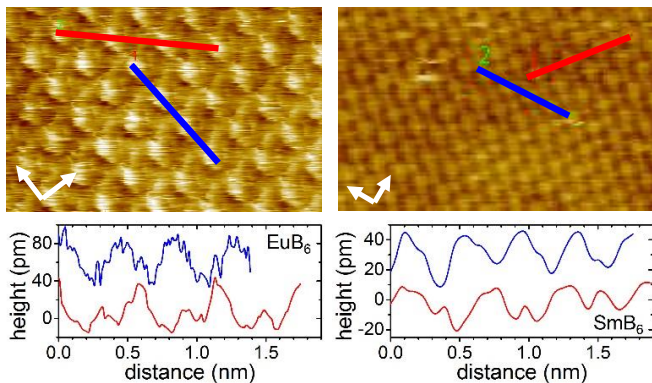


FIG. 8. Topography obtained on a Eu-terminated area ($3.4 \text{ nm} \times 2.2 \text{ nm}$) of EuB_6 (left, $V = +0.2 \text{ V}$, $I_{\text{sp}} = 0.5 \text{ nA}$) and a Sm-terminated area ($5.3 \text{ nm} \times 3.4 \text{ nm}$) of SmB_6 (right, $V = +0.2 \text{ V}$, $I_{\text{sp}} = 0.6 \text{ nA}$). Height scans along the $\langle 100 \rangle$ crystallographic directions are shown blue, and such parallel to the $\langle 110 \rangle$ directions in red. The white arrows indicate the main crystallographic directions $\langle 100 \rangle$ and $\langle 010 \rangle$.

terjacent smaller corrugations along $\langle 110 \rangle$ is pivotal for the assignment of the surface termination, yet requires sufficiently large, atomically flat and clean surface areas. However, the consistent observation of this type of surface topography on two different members of the hexaboride family makes a plausible case.

Based on DFT calculations it was suggested that the work function for a Sm-terminated surface of SmB_6 is about 2 eV , and at least twice as high on a B-terminated surface²⁹. We therefore started to investigate the tunneling barrier height Φ , which is related to the work functions of the sample and the tip (Φ_s and Φ_t , respectively). The tunneling current I decreases exponentially with increasing tip-sample distance Δz , i.e. $I(z) \propto \exp(-2\kappa \Delta z)$. The barrier height Φ can be calculated from $\kappa^2 = \frac{2m_e}{\hbar^2} \Phi$, where m_e is the bare electron mass. Figure 9 shows two curves $I(\Delta z)$ obtained on a clean B-terminated EuB_6 surface shown in the inset. The

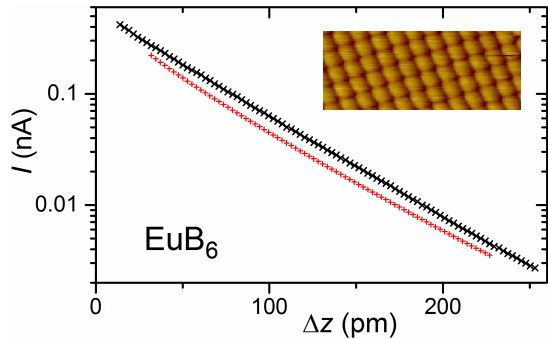


FIG. 9. Dependence of tunneling current I on change in tip-sample distance Δz taken on the B-terminated surface of EuB_6 shown in the inset (area $5 \text{ nm} \times 2 \text{ nm}$). The barrier heights correspond to 4.7 eV (black) and 5.6 eV (red).

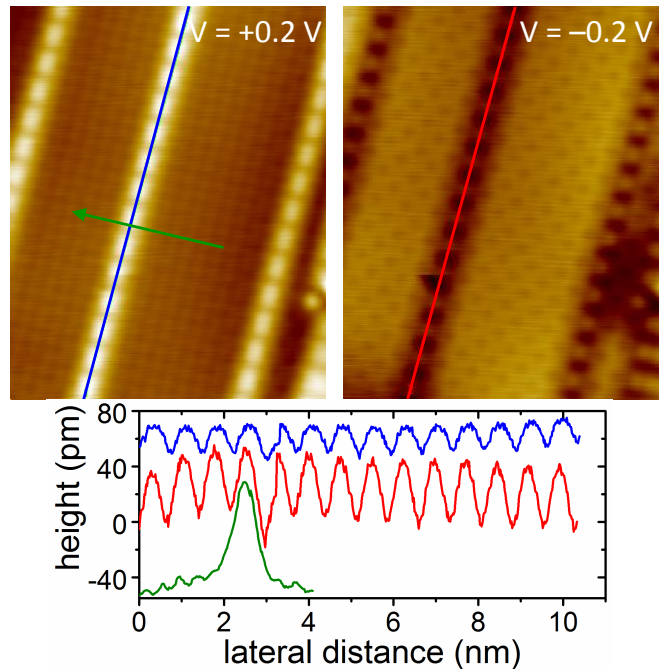


FIG. 10. Topography of an area of $8 \text{ nm} \times 10 \text{ nm}$ obtained in dual-bias mode on EuB_6 with Cr-tip. The line scans indicate a possible dimerization.

barrier heights for the two exemplary curves are $\Phi = 4.7 \text{ eV}$ and 5.6 eV , i.e. they vary by almost 1 eV . Unfortunately, because of their highly infrequent occurrence we were not able so far to measure Φ on a Eu-terminated surface. It therefore remains to be seen whether a measurement of the barrier height can help in identifying the termination of clean EuB_6 surfaces.

In the case of SmB_6 , both the investigation of slightly Gd-substituted samples with W tunneling tips and of pristine SmB_6 with Cr tips resulted in a strong suppression of the surface state⁶¹. In fact, the dI/dV curves in close proximity to magnetic defects and taken with magnetic tip are akin to spectra obtained with W tip on pristine SmB_6 at 20 K , a temperature high enough such that the surface states do not significantly contribute to the tunneling spectra. These observations are expected for topologically nontrivial surface states close to atoms carrying a sizable magnetic moment arising from an exchange interaction^{62,63}. Given this achievement in utilizing Cr tips as well as the magnetic properties of EuB_6 we also started to investigate surfaces of EuB_6 with magnetic Cr tunneling tips. One particularly intriguing example, attained in dual-bias mode for $V = \pm 0.2 \text{ V}$, is presented in Fig. 10. The dual-bias mode is important as an only partial contrast reversal for the two different V -values is observed, rendering a position adjustment of subsequently obtained images based solely on defects less reliable. This partial contrast reversal also complicates the assignment of the observed features: While the prominent bright lines seen for $V = +0.2 \text{ V}$ correspond in height (see green scan line and green height profile) to

Sm atoms, Fig. 5, and might be interpreted as Eu atoms, the same lines appear dark, i.e. as dents, for $V = -0.2$ V. We note that by utilizing a magnetic tip, contrast changes may be expected mostly on surfaces of magnetic materials. Importantly, the height profiles measured along these lines did not show any contrast reversal upon reversing V (compare the blue and red height scans in Fig. 10). The corrugations along these lines exhibit a periodicity of $2a$. Taken together, one may speculate about the formation of magnetic Eu dimers on the surface of EuB_6 . Clear of these lines, there is no obvious indication for a formation of such dimers: The green height scan exhibits corrugations (away from the aforementioned line) with distances corresponding to a . However, the apparent changes in contrast in areas between the line features upon reversal of V render this picture incomplete, at least. Clearly, measurements in magnetic fields are called for, but so far we were not able to locate such a topographic feature in our STM system with magnetic field capabilities.

IV. CONCLUSIONS

Investigating topographies on a large number of SmB_6 and EuB_6 samples revealed different surface terminations which show similarities between these two hexaborides. Such similarities are obvious for the rare-earth termi-

nated surfaces, a termination that is rather rare^{27,28} but essential when attempting an assignment of the different terminations. In addition, utilizing a dual-bias mode allowed a comparison of topographies obtained with different bias voltages on exactly identical surface areas without relying on defects. Along with the observations of step heights less than a , these observations made a reliable assignment of the rare-earth and B-terminated surfaces possible. Apart from these atomically flat terminations, we observed different line structures which may correspond to lines of rare-earth atoms on top of an otherwise B-terminated surfaces. Some of these structures exhibited intriguing properties, also if probed by magnetic tips, which warrants further study.

V. ACKNOWLEDGEMENT

We thank Silvia Seiro, Ulrich K. Rößler, Frank Steglich, Hao Tjeng and Jens Wiebe for support and discussions. Financial support from the Deutsche Forschungsgemeinschaft within the priority program SPP1666 is gratefully acknowledged. Work at Los Alamos was performed under the auspices of the U.S. Department of Energy, Office of Basic Energy Sciences, Division of Materials Science and Engineering.

-
- * steffen.wirth@cpfs.mpg.de
[†] Present address: Department of Physics and Frederick Seitz Materials Research Laboratory, University of Illinois Urbana-Champaign, Urbana, Illinois 61801, USA
- ¹ J. Etourneau and P. Hagenmuller, *Philos. Mag.* **52**, 589 (1985).
 - ² A. Berrada, J. P. Mercurio, J. Etourneau, and P. Hagenmuller, *J. Less-Common Met.* **59**, 7 (1978).
 - ³ D. P. Young, D. Hall, M. E. Torelli, Z. Fisk, J. L. Sarrao, J. D. Thompson, H. R. Ott, S. B. Oseroff, R. G. Goodrich, and R. Zysler, *Nature* **397**, 412 (1999).
 - ⁴ J. Stankiewicz, J. Sesé, G. Balakrishnan, and Z. Fisk, *Phys. Rev. B* **90**, 155128 (2014).
 - ⁵ J. M. Effantin, J. Rossatmignod, P. Burlet, H. Bartholin, S. Kunii, and T. Kasuya, *J. Magn. Magn. Mater.* **47-48**, 145 (1985).
 - ⁶ Y. S. Grushko, Y. B. Paderno, K. Y. Mishin, L. I. Molkanov, G. A. Shadrina, E. S. Konovalova, and E. M. Dudnik, *Phys. Stat. Sol. B* **128**, 591 (1985).
 - ⁷ E. E. Vainshtein, S. M. Blokhin, and Y. B. Paderno, *Sov. Phys.-Solid State* **6**, 2318 (1965).
 - ⁸ Y. Utsumi, D. Kasinathan, K.-T. Ko, S. Agrestini, M. W. Haverkort, S. Wirth, Y.-H. Wu, K.-D. Tsuei, D.-J. Kim, Z. Fisk, A. Tanaka, P. Thalmeier, and L. H. Tjeng, *Phys. Rev. B* **96**, 155130 (2017).
 - ⁹ M. Dzero, K. Sun, V. Galitski, and P. Coleman, *Phys. Rev. Lett.* **104**, 106408 (2010).
 - ¹⁰ G. Aeppli and Z. Fisk, *Comments Cond. Mat. Phys.* **16**, 155 (1992).
 - ¹¹ P. S. Riseborough, *Adv. Phys.* **49**, 257 (2000).
 - ¹² T. Takimoto, *J. Phys. Soc. Jpn.* **80**, 123710 (2011).
 - ¹³ F. Lu, J. Zhao, H. Weng, Z. Fang, and X. Dai, *Phys. Rev. Lett.* **110**, 096401 (2013).
 - ¹⁴ J. Kim, K. Kim, C.-J. Kang, S. Kim, H. C. Choi, J.-S. Kang, J. D. Denlinger, and B. I. Min, *Phys. Rev. B* **90**, 075131 (2014).
 - ¹⁵ N. Xu, P. K. Biswas, J. H. Dil, R. S. Dhaka, G. Landolt, S. Muff, C. E. Matt, X. Shi, N. C. Plumb, M. Radović, E. Pomjakushina, K. Conder, A. Amato, S. V. Borisenko, R. Yu, H. M. Weng, Z. Fang, X. Dai, J. Mesot, H. Ding, and M. Shi, *Nature Commun.* **5**, 4566 (2014).
 - ¹⁶ S. Suga, K. Sakamoto, T. Okuda, K. Miyamoto, K. Kuroda, A. Sekiyama, J. Yamaguchi, H. Fujiwara, A. Irizawa, T. Ito, S. Kimura, T. Balashov, W. Wulfhekel, S. Yeo, F. Iga, and S. Imada, *J. Phys. Soc. Jpn.* **83**, 014705 (2014).
 - ¹⁷ S. Wolgast, C. Kurdak, K. Sun, J. W. Allen, D.-J. Kim, and Z. Fisk, *Phys. Rev. B* **88**, 180405(R) (2013).
 - ¹⁸ Y. S. Eo, A. Rakoski, J. Lucien, D. Mihailiov, C. Kurdak, P. F. S. Rosa, and Z. Fisk, *Proc. Natl. Acad. Sci. USA* **116**, 12638 (2019).
 - ¹⁹ P. Hlawenka, K. Siemensemeyer, E. Weschke, A. Varykhalov, J. Sánchez-Barriga, N. Y. Shitsevalova, A. V. Dukhnenko, V. B. Filipov, S. Gabáni, K. Flachbart, O. Rader, and E. D. L. Rienks, *Nature Commun.* **9**, 517 (2018).
 - ²⁰ P. P. Baruselli and M. Vojta, *Phys. Rev. Lett.* **115**, 156404 (2015).
 - ²¹ M. Legner, A. Rüegg, and M. Sigrist, *Phys. Rev. Lett.* **115**, 156405 (2015).

- ²² M. Sundermann, H. Yavas, K. Chen, D. Kim, Z. Fisk, D. Kasinathan, M. Haverkort, P. Thalmeier, A. Severing, and L. Tjeng, *Phys. Rev. Lett.* **120**, 016402 (2018).
- ²³ V. N. Antonov, B. N. Harmon, and A. N. Yaresko, *Phys. Rev. B* **66**, 165209 (2002).
- ²⁴ C.-J. Kang, J. Kim, K. Kim, J. Kang, J. D. Denlinger, and B. I. Min, *J. Phys. Soc. Jpn.* **84**, 024722 (2015).
- ²⁵ C.-H. Min, F. Goth, P. Lutz, H. Bentmann, B. Y. Kang, B. K. Cho, J. Werner, K.-S. Chen, F. Assaad, and F. Reinert, *Sci. Rep.* **7**, 11980 (2017).
- ²⁶ Z.-H. Zhu, A. Nicolaou, G. Levy, N. P. Butch, P. Syers, X. F. Wang, J. Paglione, G. A. Sawatzky, I. S. Elfimov, and A. Damascelli, *Phys. Rev. Lett.* **111**, 216402 (2013).
- ²⁷ W. Ruan, C. Ye, M. Guo, F. Chen, X. Chen, G.-M. Zhang, and Y. Wang, *Phys. Rev. Lett.* **112**, 136401 (2014).
- ²⁸ S. Rößler, T.-H. Jang, D. J. Kim, L. H. Tjeng, Z. Fisk, F. Steglich, and S. Wirth, *Proc. Natl. Acad. Sci. USA* **111**, 4798 (2014).
- ²⁹ Z. Sun, A. Maldonado, W. S. Paz, D. S. Inosov, A. P. Schnyder, J. J. Palacios, N. Y. Shitsevalova, V. B. Filipov, and P. Wahl, *Phys. Rev. B* **97**, 235107 (2018).
- ³⁰ H. Pirie, Y. Liu, A. Soumyanarayanan, P. Chen, Y. He, M. M. Yee, P. F. S. Rosa, J. D. Thompson, D.-J. Kim, Z. Fisk, X. Wang, J. Paglione, D. K. Morr, M. H. Hamidian, and J. E. Hoffman, *Nature Phys.* **16**, 52 (2020).
- ³¹ S. Rößler, L. Jiao, D. J. Kim, S. Seiro, K. Rasim, F. Steglich, L. H. Tjeng, Z. Fisk, and S. Wirth, *Philos. Mag.* **96**, 3262 (2016).
- ³² H. Herrmann, P. Hlawenka, K. Siemensmeyer, E. Weschke, J. Sánchez-Barriga, A. Varykhalov, N. Y. Shitsevalova, A. V. Dukhnenko, V. B. Filipov, S. Gabáni, K. Flachbart, O. Rader, M. Sterrer, and E. D. L. Rienks, *Adv. Mater.* **32** (2020), doi:10.1002/adma.201906725.
- ³³ X. Zhang, S. von Molnár, Z. Fisk, and P. Xiong, *Phys. Rev. Lett.* **100**, 167001 (2008).
- ³⁴ S. Süllow, I. Prasad, M. C. Aronson, J. L. Sarrao, Z. Fisk, D. Hristova, A. H. Lacerda, M. F. Hundley, A. Vigilante, and D. Gibbs, *Phys. Rev. B* **57**, 5860 (1998).
- ³⁵ M. Pohlit, S. Rößler, Y. Ohno, H. Ohno, S. von Molnár, Z. Fisk, J. Müller, and S. Wirth, *Phys. Rev. Lett.* **120**, 257201 (2018).
- ³⁶ S. V. Ramankutty, N. de Jong, Y. K. Huang, B. Zwartsenberg, F. Masee, T. V. Bay, M. S. Golden, and E. Frantzeskakis, *J. Electron Spectrosc. Relat. Phenom.* **208**, 43 (2016).
- ³⁷ Z. Fisk, D. Johnston, B. Cornut, S. von Molnár, S. Oseroff, and R. Calvo, *J. Appl. Phys.* **50**, 1911 (1979).
- ³⁸ D. J. Kim, J. Xia, and Z. Fisk, *Nature Mater.* **13**, 466 (2014).
- ³⁹ P. F. S. Rosa and Z. Fisk, in *Crystal Growth of Intermetallics*, edited by P. Gille and Y. Grin (Berlin, Boston: De Gruyter, 2018) pp. 49–60.
- ⁴⁰ Omicron Nanotechnology GmbH, Taunusstein (Germany).
- ⁴¹ G. Schubert, H. Fehske, L. Fritz, and M. Vojta, *Phys. Rev. B* **85**, 201105(R) (2012).
- ⁴² S. Wolgast, Y. S. Eo, T. Öztürk, G. Li, Z. Xiang, C. Tinsman, T. Asaba, B. Lawson, F. Yu, J. W. Allen, K. Sun, L. Li, C. Kurdak, D.-J. Kim, and Z. Fisk, *Phys. Rev. B* **92**, 115110 (2015).
- ⁴³ M. M. Yee, Y. He, A. Soumyanarayanan, D.-J. Kim, Z. Fisk, and J. E. Hoffman, “Imaging the Kondo insulating gap on SmB₆.” (2013), arXiv:1308.1085.
- ⁴⁴ H. Miyazaki, T. Hajiri, T. Ito, S. Kunii, and S. I. Kimura, *Phys. Rev. B* **86**, 075105 (2012).
- ⁴⁵ T. Miyamachi, S. Suga, M. Ellguth, C. Tusche, C. M. Schneider, F. Iga, and F. Komori, *Sci. Rep.* **7**, 12837 (2017).
- ⁴⁶ P. Buchsteiner, F. Sohn, J. G. Horstmann, J. Voigt, M. C. Hatnean, G. Balakrishnan, C. Ropers, P. E. Blöchl, and M. Wenderoth, *Phys. Rev. B* **100**, 205407 (2019).
- ⁴⁷ K. Yoo and H. H. Weitering, *Phys. Rev. B* **65**, 115424 (2002).
- ⁴⁸ L. Jiao, S. Rößler, D. J. Kim, L. H. Tjeng, Z. Fisk, F. Steglich, and S. Wirth, *Nature Commun.* **7**, 13762 (2016).
- ⁴⁹ C. E. Matt, H. Pirie, A. Soumyanarayanan, M. M. Yee, Y. He, D. T. Larson, W. S. Paz, J. J. Palacios, M. H. Hamidian, and J. E. Hoffman, “Consistency between ARPES and STM measurements on SmB₆.” (2018), arXiv:1810.13442.
- ⁵⁰ X. Zhang, N. P. Butch, P. Syers, S. Ziemak, R. L. Greene, and J. Paglione, *Phys. Rev. X* **3**, 011011 (2013).
- ⁵¹ N. Xu, X. Shi, P. K. Biswas, C. E. Matt, R. S. Dhaka, Y. Huang, N. C. Plumb, M. Radović, J. H. Dil, E. Pomjakushina, K. Conder, A. Amato, Z. Salman, D. M. Paul, J. Mesot, H. Ding, and M. Shi, *Phys. Rev. B* **88**, 121102 (2013).
- ⁵² E. Frantzeskakis, N. de Jong, B. Zwartsenberg, Y. K. Huang, Y. Pan, X. Zhang, J. X. Zhang, F. X. Zhang, L. H. Bao, O. Tegus, A. Varykhalov, A. de Visser, and M. S. Golden, *Phys. Rev. X* **3**, 041024 (2013).
- ⁵³ W. T. Fuhrman, J. R. Chamorro, P. Alekseev, J.-M. Mignot, T. Keller, J. A. Rodriguez-Rivera, Y. Qiu, P. Nikolić, T. M. McQueen, and C. L. Broholm, *Nature Commun.* **9**, 1539 (2018).
- ⁵⁴ M. E. Valentine, S. Koohpayeh, W. A. Phelan, T. M. McQueen, P. F. S. Rosa, Z. Fisk, and N. Drichko, *Physica B* **536**, 60 (2018).
- ⁵⁵ E. S. Konovalova, Y. B. Paderno, T. Lundstrom, L. D. Finkel’shtein, N. N. Efremova, and E. M. Dudnik, *Powder Metall Met. Ceram.* **21**, 820 (1982).
- ⁵⁶ W. A. Phelan, S. M. Koohpayeh, P. Cottingham, J. A. Tutmaher, J. C. Leiner, M. D. Lumsden, C. M. Lavelle, X. P. Wang, C. Hoffmann, M. A. Siegler, N. Hal-dolaarachchige, D. P. Young, and T. M. McQueen, *Sci. Rep.* **6**, 20860 (2016).
- ⁵⁷ S. Thomas, X. Ding, F. Ronning, V. Zapf, J. Thompson, Z. Fisk, J. Xia, and P. Rosa, *Phys. Rev. Lett.* **122**, 166401 (2019).
- ⁵⁸ H. W. Zandbergen, T. J. Gortenmulder, J. L. Sarrac, J. C. Harrison, M. C. de Andrade, J. Hermann, S. H. Han, Z. Fisk, M. B. Maple, and R. J. Cava, *Physica C* **232**, 328 (1994).
- ⁵⁹ J. S. Ozcomert and M. Trenary, *Surf. Sci. Lett.* **265**, L227 (1992).
- ⁶⁰ S. Massidda, A. Continenza, T. M. de Pascale, and R. Monnier, *Z. Phys. B: Condens. Matter* **102**, 83 (1997).
- ⁶¹ L. Jiao, S. Rößler, D. Kasinathan, P. F. S. Rosa, C. Guo, H. Yuan, C.-X. Liu, Z. Fisk, F. Steglich, and S. Wirth, *Sci. Adv.* **4**, eaau4886 (2018).
- ⁶² Q. Liu, C.-X. Liu, C. Xu, X.-L. Qi, and S.-C. Zhang, *Phys. Rev. Lett.* **102**, 156603 (2009).
- ⁶³ Q.-H. Wang, D. Wang, and F.-C. Zhang, *Phys. Rev. B* **81**, 035104 (2010).